PAPER

Check for updates

Thermal decomposition of ammonium perchlorate-based molecular perovskite from TG-DSC-FTIR-MS and *ab initio* molecular dynamics†

Pengfei Zhai, [ID] ab Chengying Shi,a Shengxiang Zhao,*b Wenbin Liu,a Wenxin Wangc and Lina Yaob

(H_2dabco)[NH_4(ClO_4)$_3$] (DAP, dabco = 1,4-diazabicyclo[2.2.2]octane) is a recently synthesized ammonium perchlorate-based molecular perovskite energetic material. The high-symmetry perovskite configuration assembles the oxidant ClO_4^- and fuel H_2dabco^{2+} into a compact cubic crystal, realizing a high energy-releasing efficiency. In this study, the thermal decomposition of DAP has been investigated by thermogravimetric analysis (TG) and differential scanning calorimetry (DSC) coupled with Fourier transform infrared (FTIR) spectroscopy and mass spectroscopy (MS). The TG-DSC profiles show that DAP has an intense one-stage heat release process with a weight loss of 94.7%. The evolved gas products are identified as H_2O, CO_2, CO, HCl, HCN, NH_3, HNCO by FTIR spectrum, in which the infrared characteristic peak at 2283 and 2250 cm^{-1} is clarified not from N_2O and assigned to HNCO. The principal products are H_2O and CO_2 together with significant amounts of HCl, HCN, NH_3 in MS, while few nitrogen oxides and O_2 are detected. The experimental results show that organic components have been the prominent media for the degradation of ClO_4^-. To refine the mechanism observed in experiment, *ab initio* molecular dynamics simulations are carried out to reveal the atomistic reaction mechanisms. The decomposition of DAP starts with proton transfer from NH_4^+ and H_2dabco^{2+} to ClO_4^-. The deprotonated carbon skeleton is preferable to NH_3 in capturing O atoms, realizing a faster consumption of O atoms. Amounts of H atoms enter the environment being active free radicals, realizing an efficient autocatalytic chain propagation of degradation of ClO_4^-. The atomistic thermal decomposition reaction mechanism of DAP uncovers the role of organic components in promoting the degradation of ClO_4^-, which will help improve the synthesis strategy of molecular perovskite energetic materials with improved performance.

1. Introduction

Ammonium perchlorate (AP), as a powerful oxidant, can produce a self-sustaining deflagration reaction when mixed with fuel, and is the most commonly used energetic component of solid composite propellants.[1] The deflagration performance of a propellant is directly related to the complex thermal decomposition mechanism of AP. People have been committed to enhancing the combustion rate by reducing the high-temperature decomposition (HTD) temperature and increasing the apparent heat release of AP.[1–3] One of the most commonly used methods is nano-additives, whose catalytic

activity can effectively reduce the HTD temperature of AP. The two-stage thermal decomposition reaction of AP can be merged into one-stage one with appropriate amount of addition, so the heat release of AP is more concentrated. Among various nano-additives, carbon materials such as carbon nanotubes and graphene that can combust exothermically like a fuel with oxidizing gas products generated from the thermal decomposition of AP, realize a much higher apparent heat release (>3000 J g^{-1}).[2,3] As the amount of addition is further increased, the thermal decomposition temperature can be further reduced, but the heat release is also reduced, indicating that the main heat source is still from AP. Therefore, although the combustion heat of carbon materials contributes to the higher heat release, the additional oxygen-consuming reaction, which greatly promote the thermal decomposition of AP, should be the main reason.

Another method is crystal engineering, which assembles AP molecules with appropriate ligand molecules at the molecular level to obtain the desired improvement. Cocrystal is a new crystal formed by combining two or more known neutral

aXi'an High-tech Research Institute, Xi'an 710025, People's Republic of China. E-mail: zhaipengfei104@163.com; shichengying104@163.com

bXi'an Modern Chemistry Research Institute, Xi'an 710065, People's Republic of China. E-mail: xamcri@126.com

cSichuan Honghua Industrial Co., Ltd., Chengdu 611130, People's Republic of China

molecules at a certain stoichiometric ratio through non-bonding interaction.[4] Three cocrystals of AP and crown ethers – AP/18-crown-6, AP/benzo-18-crown-6 and AP/dibenzo-18-crown-6, have been synthesized.[5] The last two cocrystals have a single obvious exothermic process at a lower temperature, with heat release increased to 1304.2 J g^{-1} and 1488.4 J g^{-1}. Looking into the spatial configuration, the large and stretched ring skeletons of crown ethers are packed disorderly and thus the space of crystal is filled with many free volumes. Consequently, the crystal density is decreased far below that of AP and so is the corresponding energy density. Therefore, although the heat release of the cocrystal is increased relative to AP, which can be attributed to the catalytic effect of organic component and its exothermic combustion, the low crystal density limits the heat release to a low level.

Different from the direct "mixing" of cocrystal, molecular perovskites assemble molecules by introducing organic molecular unit into the perovskite architecture.[6] (H_2dabco)[NH_4(ClO_4)$_3$] (DAP, dabco = 1,4-diazabicyclo[2.2.2]octane) introduces organic cation H_2dabco^{2+} as A component, with NH_4^+ cation as B component and ClO_4^- anion as X component, to assemble a high symmetry ternary perovskite ABX$_3$ structure,[7,8] which realize a homogeneous mixing of fuel and oxidant at the molecular level.[9] The organic component H_2dabco^{2+} cation also has a ring skeleton but small and compact. And the electrostatic interaction between cation and anion is stronger than neutral molecules. Thus, the compact cubic crystal has a density close to AP, far above that of cocrystal. Furthermore, DAP is easier to be modified by replacing A, B or X component.[10,11] Compared with AP, DAP has a lower thermal decomposition temperature and a single intense exothermic process, and its heat release has reached the level of nano-additives of carbon materials (>3000J g^{-1}).[12,13] These lay a good foundation for the further modification and application of DAP.[14,15]

The catalytic performance of nano-additives depends on the effective contact area and the number of active sites with AP. Simply mixing their nanoparticles or making them porous nanocomposites, in essence, is physically mixed and subject to the strength of interaction and the uniformity of dispersion. The cocrystals of AP and crown ethers suffer from low crystal density, so more types of cocrystal need to be synthesized with more suitable ligand molecules. DAP seemingly integrate the advantages of all above methods. More importantly, it is evident that the organic components play a key role in the thermal decomposition of AP, which need to be further revealed by studying the thermal decomposition mechanism of DAP.

The structure changes of DAP have been studied by *in situ* FTIR in heating process.[13] The cage skeleton constructed by NH_4^+ and ClO_4^- ions decomposes before the organic moiety and determines the decomposition process. The combustion flames photographed with high speed photography and the gas release process recorded by TG-FTIR show a fierce one-stage energy-releasing effect of DAP.[12] However, the chemical reactions during the decomposition process of DAP still remain unclear. The infrared characteristic peaks of gas products in the FTIR spectra show significant changes compared with AP.[12] But the gas composition has not been identified, nor has the reason

been given for these changes. To examine the thermal decomposition reaction process of DAP, thermogravimetric analysis and differential scanning calorimetry coupled with Fourier transform infrared spectroscopy and mass spectroscopy (TG-DSC-FTIR-MS) experiments and *ab initio* molecular dynamics simulations are carried out to identify the evolved gas products. The concentration–time profile of gas products gives clues about the elementary reactions,[16] while the *ab initio* molecular dynamics simulations trace the breaking and formation of bond on atomic scale.[17–19] Theoretical calculations can well make up for the insufficiency of macroscopic experiments on the exploration of microscopic mechanism, while the corresponding results of macroscopic experiments verify the reliability of theoretical calculations.

2. Experimental and computational details

2.1 Experiments

2.1.1 Sample preparation. DAP samples are prepared according to the method proposed by Deng *et al.*[12] and purified to >99%.

2.1.2 Powder X-ray diffraction measurements. The Powder X-ray diffraction (PXRD) patterns of prepared samples are collected by a Philips X'Pert Pro X-ray diffractometer (PANalytical, Holland). The PXRD patterns of crystal model are simulated with the reflex module in Materials Studio 8.0.[20] Cu is selected as the target and the scanning range is 5–50° with a step-width of 0.02°.

2.1.3 TG-DSC-FTIR-MS measurements. Place ~2 mg of samples in an aluminum oxide crucible and load it on the Netzsch 449C TG-DSC synchronous thermal analyzer. Heat the samples from 30 to 500 °C at the heating rate of 10 °C min^{-1}. High-purity argon is used as the purge gas, and the evolved gas products are transferred into the coupled QMS403 quadrupole mass spectrometer and Nicolet 5700 infrared spectrometer at a flow rate of 25 ml min^{-1}. The FTIR spectral is recorded in the range of 4000–650 cm^{-1} with a resolution of 4 cm^{-1}. The FTIR gas pool is maintained at 200 °C, while the tube connecting thermal analyzer, mass spectrometer and infrared spectrometer is maintained at 210 °C. The electron impact ionization energy of mass spectrometer is 70 eV. Operations of some characterization items can refer to the literature.[21–25]

2.2 *Ab initio* calculations

The lattice parameters of DAP (CCDC No. 1528108) determined by Chen *et al.*[9] are used to construct the crystal model. The spatial configuration and molecular composition of DAP crystal are shown in Fig. 1. DAP molecule is composed of five elements – C, H, O, N, and Cl. They are described by first-principles pseudopotentials constructed by projection augmented waves.[26,27] C 2s2p, H 1 s, N 2s2p, O 2s2p, Cl 3s3p are considered as valence state. The exchange correlation functional adopts the generalized gradient estimation (GGA) in the form of Perdew, Burke, and Ernzerhof formulation (PBE).[28] The cutoff energy of the plane wave basis set is set to 600 eV. Grimme's DFT-D2 (ref.
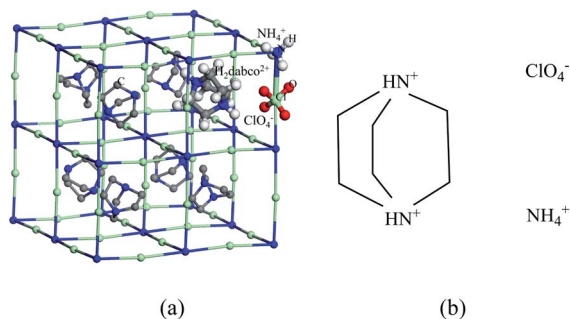
Fig. 1 Spatial configuration (a) and molecular composition (b) of DAP. C, H, N, O, Cl are represented by gray, wight, blue, red, and green-yellow balls respectively. For clarity, only one ClO_4^- is shown with O atoms and one H_2dabco^{2+} and NH_4^+ are shown with H atoms.

29) method is used to correct long-range dispersion interaction. Considering that the DAP unit cell contains 336 atoms, which is bigger than the supercell of common energetic material crystals used for *ab initio* molecular dynamics simulations,[30] the DAP unit cell is large enough to be used as the crystal model for *ab initio* molecular dynamics simulations with single Gamma point. In order to verify the applicability of the single Gamma point calculation to the DAP unit cell, the conjugate gradient method was used to perform complete structural relaxation (lattice and atom relaxed at the same time). The electronic iteration and ion relaxation convergence criteria are set to 1×10^{-7} and 1×10^{-6} eV. The optimized lattice parameters are in good agreement with the experimental values (see Table 1), which proves the reliability of the DAP calculation. Furthermore, the consistency of gas products obtained by experiment and calculation also verify the reliability of the calculation method. The Verlet algorithm is used for molecular dynamics integration with a time-step of 0.25 fs. The Nose–Hoover thermostat is used to realize a canonical ensemble (NVT). The optimized DAP unit cell is firstly relaxed at 300 K for 0.5 ps to eliminate the unreasonable internal stress. After that, the temperature is rapidly increased to 3000 K within 0.25 ps and the relaxed DAP unit cell is maintained at the temperature for 9 ps to be fully decomposed. In order to trace the evolution of product clusters, the cluster analysis method proposed by Lu *et al.*[30] is used. If the distance between two atoms is less than 1.33 times the normal covalent bond length[31] and maintained for 25 fs (with hydrogen atoms bonded) or 50 fs (without

hydrogen atoms bonded),[32] the two atoms are considered bonded.

For comparison, the decomposition of AP is also simulated. The lattice parameters of AP (CCDC No. 725655) determined by Kumar *et al.*[33] are used to construct the crystal model. Since the AP unit cell contains only 40 atoms, a $2 \times 1 \times 1$ supercell constructed from the optimized unit cell is used for the sing le Gamma point *ab initio* molecular dynamics simulation, while all other parameter settings are consistent with that of DAP.

3. Results and discussion

3.1 Experimental results

PXRD are often used for structural analysis. Pure substances have unique spatial configurations and crystal plane arrangements, which are depicted by certain diffraction peaks in PXRD figures like fingerprints. Fig. 2 shows the PXRD peaks of the prepared DAP samples and the DAP crystal model. The distribution of diffraction peaks of samples is consistent with that of crystal model, indicating that DAP has been successfully synthesized. The TG-DSC curves in Fig. 3 depicts the weight loss and energy release characteristics of DAP in the thermal decomposition process. The mass change of DAP samples starts at 292.7 °C and end at 402.6 °C with a weight loss of 94.7%. The weight loss curve has only one steep downward stage and so there is a single sharp exothermic peak on the DSC curve. The exothermic peak temperature is 381.8 °C. The thermal decomposition of DAP shows a rapid and concentrated one-stage heat release process different from that of AP.[34–36]

The infrared characteristic peaks in the FTIR spectrum correspond to certain characteristic vibrations of gas molecules which are fingerprints to identify the chemical species of gas products. By comparing the infrared characteristic peaks of gas products of DAP at 381.8 °C (Fig. S1(b)†) with the standard gas infrared data provided in HITRAN2016 molecular spectroscopic database (Fig. S1(a)†),[37] the gas components can be clearly identified to include CO_2, CO, H_2O, HCl, HCN, NH_3. It should be noted that high temperature will broaden the infrared characteristic peaks of some gases, but the central locations are almost unchanged (Fig. S2†). Since the temperature of FTIR gas cell is only maintained at 210 °C, for the infrared characteristic peaks not overlapped, the temperature-induced uncertainty can be ignored. More difficult is the identification of HNCO and N_2O, which are the key to understanding the thermal decomposition mechanism of DAP. N_2O is a symbolic gas product for

Table 1 Lattice parameters of DAP and AP

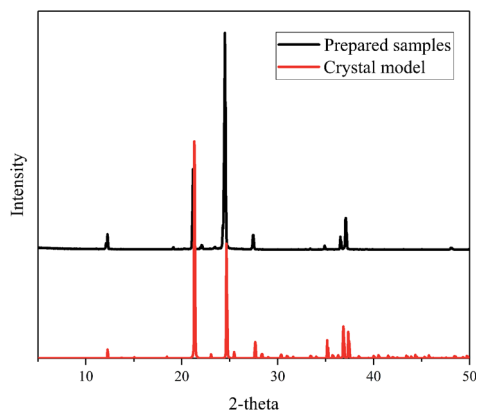| Lattice parameters	DAP			AP		
	Exp.[a]	Comp.	Relative error/%	Exp.[b]	Comp.	Relative error/%
a/Å	14.426	14.249	−1.23	9.176	8.779	−4.33
b/Å	—	—	—	5.797	5.976	3.09
c/Å	—	—	—	7.420	7.224	−2.64
ρ/(g cm^{-3})	1.905	1.977	3.78	1.977	2.059	4.15

[a] Cited from ref. 7. [b] Cited from ref. 24.

Fig. 2 PXRD of crystal model and prepared samples for DAP (red line for crystal model, black line for prepared samples).
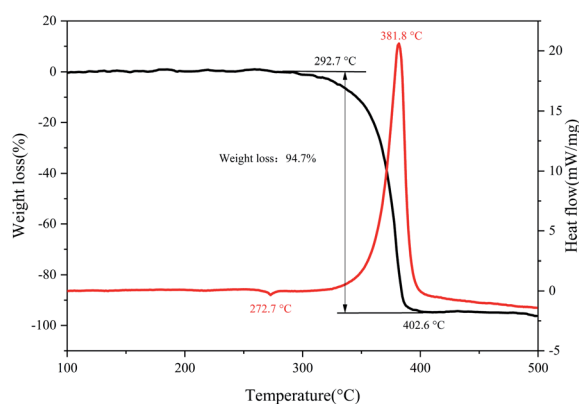

Fig. 4 Evolution of gas products from FTIR spectrum for DAP decomposed at the heating rate of 10 °C min^{-1}.

Fig. 3 Weight loss and heat release for DAP decomposed at the heating rate of 10 °C min^{-1} (black line for TG, red line for DSC).

Fig. 5 Evolution of product fragments from MS for DAP decomposed at the heating rate of 10 °C min^{-1}.

AP and has the strongest infrared characteristic peak at 2239 and 2204 cm^{-1} (Fig. S3†). For DAP, the infrared characteristic peak at 2283 and 2250 cm^{-1} (Fig. S1(b)†) is also the strongest and has a similar profile with that of N_2O. Considering that DAP contains the same component with AP, it is easy to jump to conclusions and identify it as N_2O. However, the latter has an obvious shift to high wavenumber region, which is more consistent with that of HNCO. At the same time, the second characteristic peak of N_2O at 1303 and 1269 cm^{-1} is absent, while that of HNCO appears at 3525 cm^{-1}. Furthermore, the infrared characteristic peaks of CO_2 and HNCO are partially overlapped in the range of 2200–2400 cm^{-1}, which is consistent with the FTIR spectrum in.[16,38,39] The infrared characteristic peaks of CO_2 and N_2O are clearly not overlapped even under high temperature (Fig. S4†), which is consistent with the FTIR spectrum in.[16,39] Therefore, the infrared characteristic peak at 2283 and 2250 cm^{-1} is assigned to HNCO. The gas products in the thermal decomposition process of DAP include CO_2, CO, H_2O, HCl, HCN, NH_3, HNCO (Fig. 4).

The concentration–time profiles obtained from mass spectrum show the evolution of product fragments. In Fig. 5, the product fragments all concentrate at 381.8 °C, indicating
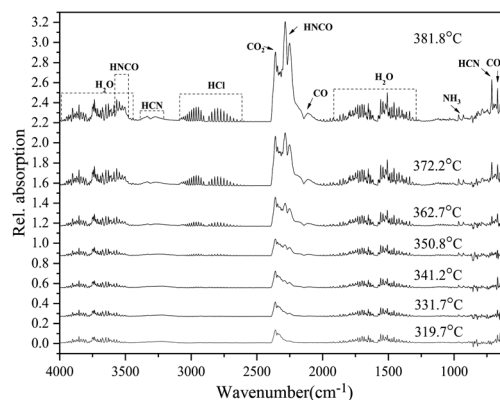
a fierce thermal decomposition of DAP. It should be noted that the relative abundance of O_2 ($m/z = 32$) shows a negative increase at 381.8 °C. O_2 is a common gas product in the thermal decomposition process of AP.[40] The rupture of Cl–O bond will produce many oxygen free radicals like O, O_2 and O_3. Their strong oxidation activity can oxidize NH_3 into various nitrogen oxides, which is a representation of oxidizing ability of AP. The negative increase of O_2 here indicates that there is no O_2 newly generated, but the O_2 from background gases is consumed by certain gas products. Considering that there is no fragments peak of CO ($m/z = 28$) in the mass spectrum, but the infrared characteristic peaks of CO do appear in the FTIR spectrum, it can be speculated that CO has been oxidized by O_2 in mass spectrometer. On the other hand, the absence of O_2 indicates that there may be few higher-order oxygen radicals generated in the thermal decomposition process of DAP. The single O radicals generated first from the rupture of Cl–O bond are quickly consumed, so there is no enough time for them to gather to higher-order oxygen radicals.

The chemical species of product fragments at 381.8 °C are deduced from the mass-to-charge ratio (Table 2). Combined with FTIR spectrum, CO_2, H_2O, HCl, HCN, NH_3 are confirmed to sole principal species, but there are no mass-to-charge ratios

Table 2   Assignment of product fragments for DAP decomposed at 381.8 °C

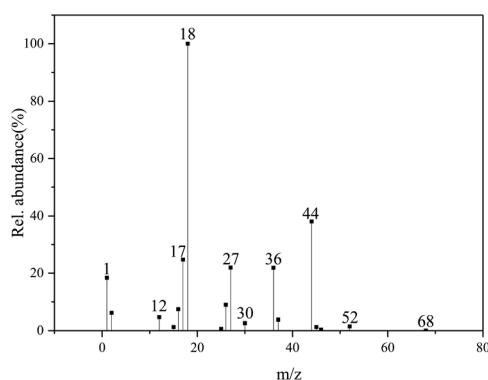| m/z	Ion current/×10^{-10} A	Species	m/z	Ion current/×10^{-10} A	Species
1	1.011	H	30	0.143	NO, CH_2O
2	0.337	H_2	36	1.202	HCl
12	0.256	C	37	0.210	^{37}Cl
15	0.070	NH, CH_3	44	2.091	CO_2, N_2O
16	0.408	O, NH_2, CH_4	45	0.07	HCO_2, HN_2O
17	1.359	OH, NH_3	46	0.021	NO_2
18	5.493	H_2O, NH_4	52	0.083	$HClO$
25	0.036	C_2H	68	0.003	$HClO_2$
26	0.492	CN			
27	1.206	HCN			

Fig. 6   Fragments of gas products from MS for DAP decomposed at 381.8 °C.

correspond to CO and HNCO. The absence of CO has been explained above. One possible reason for the absence of HNCO is that HNCO has been ionized to H_2NCO^+ (m/z = 44) by adding H^+, who will be covered by the fragments peak of CO_2, since there are many fragments of H^+ in the mass spectrometer. In the molecular dynamics simulation, HNCO eventually exists in the form of HNCO ⇆ H_2NCO, indicating that it is easy for HNCO to capture another H. But high-precision mass spectrometry experiments are needed to confirm this. The relative abundance of primary product fragments is shown in Fig. 6. H_2O has the

largest abundance more than twice the second largest one of CO_2, indicating a large amount of O atoms decomposed from ClO_4^- have been captured by H atoms. In the decomposition of AP, H_2O is also aprincipal product.[40] The decomposition of AP starts with the proton transfer from NH_4^+ to ClO_4^- and $HClO_4$ is degraded from high-order oxychloride or oxyacid to low-order ones, in which H atoms play an important role in the autocatalytic chain propagation.[41] Since the cage skeleton constructed by NH_4^+ and ClO_4^- ions determines the decomposition process of DAP,[13] it can be speculated that the decomposition also start with the proton transfer from NH_4^+ to ClO_4^-. The presence of HClO and $HClO_2$ indicates that the degradation of $HClO_4$ is also an autocatalytic chain propagation from high-order oxychloride or oxyacid to low-order ones. More abundant H_2O origins from the organic components and higher proportion of ClO_4^-. N_2O has been identified not included in the gas products by FTIR spectrum. Although there are fragments peaks with m/z = 30 and 46, which possibly belong to NO and NO_2 respectively, their abundance is too small. Therefore, nitrogen oxides, which are the main oxygen-consuming products in the decomposition of AP,[34,35] have been replaced by carbon oxides. NH_3, HCN and HCl have close and significant relative abundance. NH_3 comes from the deprotonated NH_4^+. HCl is a symbolic product for the degradation of ClO_4^-. And HCN comes from the polyazine unit in the carbon-nitrogen heterocycle of H_2dabco^{2+}, which is a common decomposition product of carbon-nitrogen
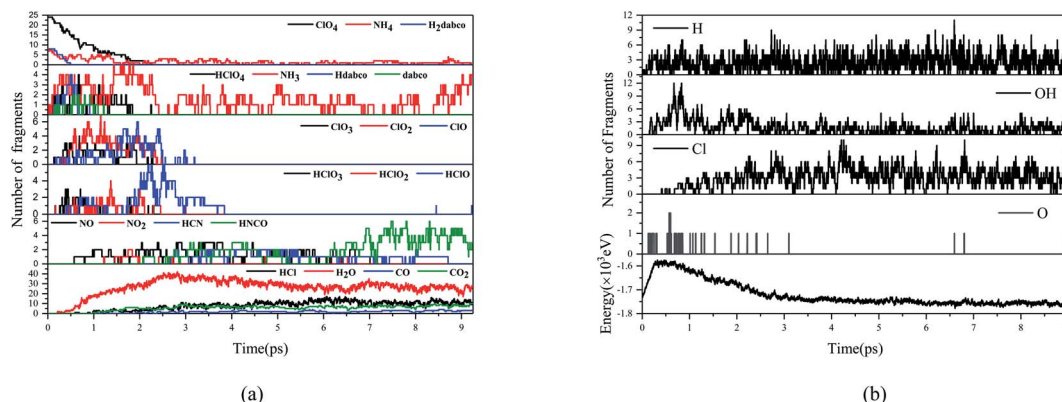

Fig. 7   Evolution of key chemical species (a), free radicals and potential energy (b) for DAP decomposed at 3000 K.
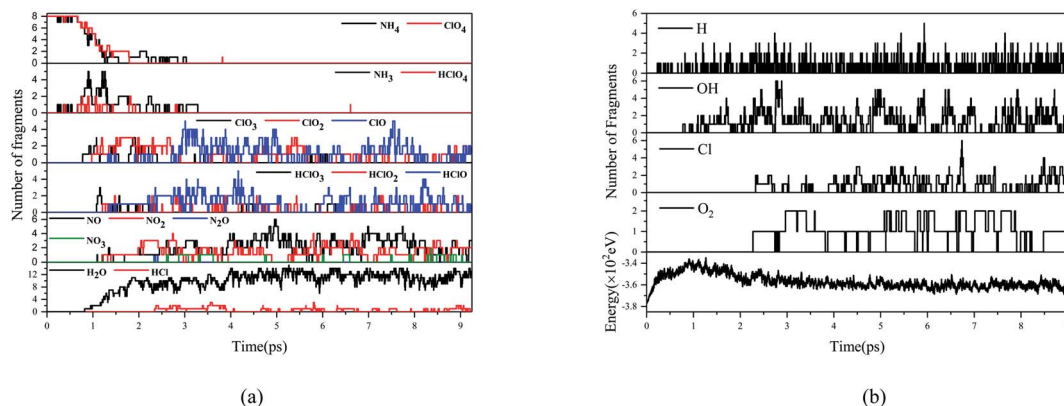
Fig. 8 Evolution of key chemical species (a), free radicals and potential energy (b) for AP decomposed at 3000 K.

heterocyclic molecules like RDX, HMX and CL-20.[16,42] HNCO often accompanies with HCN, which is derived from the amide unit after the carbon skeleton is oxidized by O atoms. Another important gas product generated from the decomposition of carbon-nitrogen heterocycle is CH_2O. But it cannot be identified in the FTIR spectrum. The relative abundance of fragments with $m/z = 30$ is also much smaller than that of CO_2. This indicates that H_2dabco^{2+} may lose H atoms first before the ring skeleton breaks or is oxidized by O atoms. So H_2dabco^{2+} is more stable than its precursor of dabco under the confinement of cage skeleton.

In the thermal decomposition process of ClO_4^-, the highly reactive transient radicals ClO_x ($x = 1$–3) can only survive for a very short time and few of them can escape in the form of gas. Therefore, they can hardly be detected by FTIR and quadrupole electron impact MS (the MS used in the paper).

In the paper,[36] the author summarized the detection results of various FTIR and MS methods on the thermal decomposition products of AP. Only the state-of-the-art single vacuum ultraviolet (VUV) photoionization coupled with reflectron time-of-flight mass spectrometry (PI-ReTOF-MS) can detect all ClO_x ($x = 1$–3) radicals, though the intensity of signal is much weaker than that of primary gas products. The FTIR and quadrupole electron impact MS can hardly detect the ClO_x ($x = 1$–3) radicals.

In the following simulations, the reason why ClO_x ($x = 1$–3) seem to have good half-lives is that they are transformed continuously from ClO_4^-. When ClO_4^- is degraded completely, ClO_x ($x = 1$–3) disappear almost at the same time. Therefore, a single ClO_x can only survive for a very short time. Only HClO exists for a certain time after all ClO_x ($x = 1$–4) and $HClO_x$ ($x = 2$–4) disappear, so it has a relatively good half-life. This is why for the only two $HClO_x$ detected by MS, the intensity of signal of HClO is much stronger than that of $HClO_2$, but is still much weaker than that of primary gas products. This is consistent with detection results of AP, in which only HClO can be detected even with PI-ReTOF-MS.

3.2 *Ab initio* calculation results

Fig. 7 and 8 show the evolution of prominent atomic clusters and potential energy respectively for DAP and AP decomposed

at 3000 K. The chemical species for AP include NH_3, $HClO_x$ ($x = 1,2,3,4$), ClO_x ($x = 1,2,3$), NO_x ($x = 1,2,3$), N_2O, H_2O, HCl, while for DAP including NH_3, hdabco, dabco, $HClO_x$ ($x = 1,2,3,4$), ClO_x ($x = 1,2,3$), NO_x ($x = 1,2$), HCN, HNCO, H_2O, HCl, CO_x ($x = 1,2$). The products composition and content are consistent with the thermal decomposition experiments of AP and DAP, which verifies the reliability of *ab initio* molecular dynamics simulations. The presence of CO and HNCO verifies the experimental inference. When the temperature is heated to 3000 K, DAP decomposes quickly, while AP does not until 0.662 ps. AP has been heated to its HTD reaction, whose onset temperature is higher than that of DAP. The first appearance of NH_3 and $HClO_4$ indicates that the thermal decomposition of AP and DAP both begin with the proton transfer from NH_4^+ to ClO_4^-. For DAP, the cage skeleton collapses soon after the proton transfer and loses its confinement on h_2dabco^{2+}. h_2dabco^{2+} is deprotonated to $Hdabco^+$ and dabco almost simultaneously with the proton transfer, so H_2dabco^{2+} is also an important proton donor. It is worth mentioning that H_2dabco^{2+} seemingly prefers to lose the C-terminal H atoms instead of N-terminal H atoms, since there are more HNCO than HCN in the products. In fact, it's easy for H atoms to escape short-lived from X–H bond under thermal stimulation due to its minor mass. When losing H atoms, the exposed C atoms are easier to be oxidized by O atoms than N atoms, which produces –CO– groups instead of –NO– groups on the ring skeleton. Therefore, the C atoms have superiority over N atoms in the competition for O atoms. Although the decomposition starts from between NH_4^+ and ClO_4^-, only few nitrogen oxides generated and a significant amount of NH_3 exit till the end of reaction, which is opposite to that of AP. The degradation of $HClO_4$, which gradually changes from higher-order oxychloride or oxyacid to low-order ones, is a process of losing O atoms. When the cage skeleton collapsed, H_2dabco^{2+} loses H atoms first. Part of H atoms transfer to ClO_4^-, while most of them enter the environment. The H atoms in the environment is maintained at a high level, which realize a more efficient autocatalytic chain propagation process, that is, a faster consumption of O atoms. This can be verified by the evolution of oxygen radicals. There are mainly single O radicals for DAP but O_2 radicals for AP in the environment, indicating that the O atoms are consumed much faster in the thermal

decomposition process of DAP, so there is no enough time for them to gather to form higher-order oxygen radicals. The first appearance of H_2O means that O atoms are first captured by H atoms. The number of OH radicals rise rapidly until the appearance of Cl atoms, which will be captured by H atoms to produce HCl. From the perspective of energy release, the inflection point of potential energy of AP lags behind and there is a second-stage energy release process when Cl atoms appear. On the one hand, NH_3 is relatively inert and it requires more energy to break N–H bond; on the other hand, breaking the last Cl–O bond to produce Cl atoms also requires more energy. However, it is much easier for C–H bond to break in DAP, and the rapid oxygen-consuming process accumulates enough heat to make the last Cl–O bond break earlier. Therefore, the appearance of Cl atoms is almost at the inflection point and the potential energy release is more concentrated and smoothed. The main energy release of DAP is finished when oxychloride or oxyacid are degraded completely (approach 3 ps), but the energy release of AP is insufficient due to the incomplete degradation of $HClO_4$.

4. Conclusions

In summary, the thermal decomposition of DAP starts with proton transfer from NH_4^+ and H_2dabco^{2+} to ClO_4^-, however, the degradation pathway of ClO_4^- has been changed by organic components compared with that of AP. Firstly, the deprotonated carbon skeleton is preferable to NH_3 in capturing O atoms, which realizes a faster consumption of O atoms. Secondly, amounts of H atoms released from H_2dabco^{2+} enter the environment being active free radicals, realizing an efficient autocatalytic chain propagation of degradation of ClO_4^-. Therefore, the generation of gas products is fast and concentrated, and so is the energy release. Molecular perovskites have provided a novel assembly strategy for energetic molecules that can achieve high energy release.

Conflicts of interest

There are no conflicts of interest to declare.

Notes and references

1 Q. L. Yan, F. Q. Zhao, K. K. Kuo, X. H. Zhang, S. Zeman and L. T. DeLuca, *Catalytic effects of nano additives on decomposition and combustion of RDX-, HMX-, and AP-based energetic compositions*, Elsevier Ltd, 2016, vol. 57.

2 J. Chen, S. He, B. Huang, L. Zhang, Z. Qiao, J. Wang, G. Yang, H. Huang and Q. Hao, *Appl. Surf. Sci.*, 2018, **457**, 508–515.

3 W. Zhang, Q. Luo, X. Duan, Y. Zhou and C. Pei, *Mater. Res. Bull.*, 2014, **50**, 73–78.

4 R. A. Wiscons and A. J. Matzger, *Cryst. Growth Des.*, 2017, **17**, 901–906.

5 M. Cheng, X. Liu, Q. Luo, X. Duan and C. Pei, *CrystEngComm*, 2016, **18**, 8487–8496.

6 G. Kieslich and A. L. Goodwin, *Mater. Horiz.*, 2017, **4**, 362–366.

7 L. Cao, X. Liu, Y. Li, X. Li, L. Du, S. Chen, S. Zhao and C. Wang, *Front. Phys.*, 2021, **16**, 33201.

8 N. Mercier, S. Poiroux, A. Riou and P. Batail, *Inorg. Chem.*, 2004, **43**, 8361–8366.

9 S. L. Chen, Z. R. Yang, B. J. Wang, Y. Shang, L. Y. Sun, C. T. He, H. L. Zhou, W. X. Zhang and X. M. Chen, *Sci. China Mater.*, 2018, **61**, 1123–1128.

10 Y. Shang, Z.-H. Yu, R.-K. Huang, S.-L. Chen, D.-X. Liu, X.-X. Chen, W.-X. Zhang and X.-M. Chen, *Engineering*, 2020, **6**, 1013–1018.

11 Y. Shang, R. Huang, S. Chen, C. He, Z. Yu, Z. Ye, W. Zhang and X.-M. Chen, *Cryst. Growth Des.*, 2020, **20**, 1891–1897.

12 P. Deng, H. Wang, X. Yang, H. Ren and Q. Jiao, *J. Alloys Compd.*, 2020, **827**, 154257.

13 J. Zhou, L. Ding, F. Zhao, B. Wang and J. Zhang, *Chin. Chem. Lett.*, 2019, **31**, 554–558.

14 K. Han, X. Zhang, P. Deng, Q. Jiao and E. Chu, *Vacuum*, 2020, **180**, 109572.

15 Q. Jia, X. Bai, S. Zhu, X. Cao, P. Deng and L. Hu, *J. Energ. Mater.*, 2020, **38**, 377–385.

16 T. B. Brill, *Combust. Flame*, 1985, **62**, 213–224.

17 Q. An, W. G. Liu, W. A. Goddard, T. Cheng, S. V. Zybin and H. Xiao, *J. Phys. Chem. C*, 2014, **118**, 27175–27181.

18 Z. Lu, Y. Xiong, X. Xue and C. Zhang, *J. Phys. Chem. C*, 2017, **121**, 27874–27885.

19 L. Meng, Z. Lu, X. Wei, X. Xue, Y. Ma, Q. Zeng, G. Fan, F. Nie and C. Zhang, *CrystEngComm*, 2016, **18**, 2258–2267.

20 P. Zhai, C. Shi, S. Zhao, Z. Mei and Y. Pan, *RSC Adv.*, 2019, **9**, 19390–19396.

21 M. Wu, Y. Chen, H. Lin, L. Zhao, L. Shen, R. Li, Y. Xu, H. Hong and Y. He, *Water Res.*, 2020, **181**, 115932.

22 Y. Long, G. Yu, L. Dong, Y. Xu, H. Lin, Y. Deng, X. You, L. Yang and B. Q. Liao, *Water Res.*, 2021, **189**, 116665.

23 Y. Xu, Y. Xiao, W. Zhang, H. Lin, L. Shen, R. Li, Y. Jiao and B. Q. Liao, *J. Membr. Sci.*, 2021, **618**, 118726.

24 R. Li, J. Li, L. Rao, H. Lin, L. Shen, Y. Xu, J. Chen and B. Q. Liao, *J. Membr. Sci.*, 2021, **619**, 118790.

25 Y. Liu, L. Shen, H. Lin, W. Yu, Y. Xu, R. Li, T. Sun and Y. He, *J. Membr. Sci.*, 2020, **612**, 118378.

26 P. E. Blöchl, *Phys. Rev. B: Condens. Matter Mater. Phys.*, 1994, **50**, 17953–17979.

27 D. Joubert, *Phys. Rev. B: Condens. Matter Mater. Phys.*, 1999, **59**, 1758–1775.

28 J. P. Perdew, K. Burke and M. Ernzerhof, *Phys. Rev. Lett.*, 1996, **77**, 3865–3868.

29 A. Allouche, *J. Comput. Chem.*, 2012, **32**, 174–182.

30 Z. Lu, Y. Xiong, X. Xue and C. Zhang, *J. Phys. Chem. C*, 2017, **121**, 27874–27885.

31 P. Pyykkö and M. Atsumi, *Chem.–Eur. J.*, 2009, **15**, 186–197.

32 M. R. Manaa, E. J. Reed, L. E. Fried and N. Goldman, *J. Am. Chem. Soc.*, 2009, **131**, 5483–5487.

33 D. Kumar, I. P. S. Kapoor, G. Singh and R. Fröhlich, *Int. J. Energ. Mater. Chem. Propul.*, 2010, **9**, 549–560.

34 L. Mallick, S. Kumar and A. Chowdhury, *Thermochim. Acta*, 2015, **610**, 57–68.

35 L. Mallick, S. Kumar and A. Chowdhury, *Thermochim. Acta*, 2017, **653**, 83–96.

36 S. Góbi, L. Zhao, B. Xu, U. Ablikim, M. Ahmed and R. I. Kaiser, *Chem. Phys. Lett.*, 2018, **691**, 250–257.

37 I. E. Gordon, L. S. Rothman, C. Hill, *et al.*, *J. Quant. Spectrosc. Radiat. Transfer*, 2017, **203**, 3–69.

38 M. S. Lowenthal, R. K. Khanna and M. H. Moore, *Spectrochim. Acta, Part A*, 2002, **58**, 73–78.

39 Y. Oyurni, B. Brill and L. Rheingold, *J. Phys. Chem.*, 1985, 2309–2315.

40 V. R. P. Verneker and J. N. Maycock, *J. Chem. Phys.*, 1967, **47**, 3618–3621.

41 V. V. Boldyrev, *Thermochim. Acta*, 2006, **443**, 1–36.

42 D. G. Patil and T. B. Brill, *Combust. Flame*, 1993, **92**, 456–458.